J Nanostruct 15(4): 2517-2527, Autumn 2025

RESEARCH PAPER

Preparation and Characterization of Hybrid TiO_2-MgO Nanoparticles Supported on Reduced Graphene Oxide (TiO_2-MgO/rGO (TMG)) as Antibacterial and Antifungal Agent

Bakhtiyor Khasanov [1]*, Sherzod Gaybullaev [2], Musharraf Mukhammadieva [1], Shahlo Akhamdjonova [3], Mehriniso Qoyilova [4], Gulnora Rakhimova [5], Oygul Rakhimova [5], Urinboy Kuryozov [6], Zaynobiddin Khakimov [7], Sayyora Akhmedova [8], Abseit Rustemov [9], Dilshodxon Kodirova [10], Rasulov Ilkhom Inamovich [11]

[1] *Bukhara State Medical Institute named after Abu Ali ibn Sino, Bukhara, Uzbekistan*

[2] *Samarkand State Medical University, Samarkand, Uzbekistan*

[3] *Fergana Medical Institute of Public Health, Fergana, Uzbekistan*

[4] *Bukhara State Pedagogical Institute, Bukhara, Uzbekistan*

[5] *Tashkent Pharmaceutical Institute, Tashkent, Uzbekistan*

[6] *Urgench State University named after Abu Rayhan Beruni, Urgench, Uzbekistan*

[7] *Andijan State Medical Institute, Andijan, Uzbekistan*

[8] *Tashkent State Medical University, Tashkent, Uzbekistan*

[9] *Chirchik State Pedagogical University, Chirchik, Uzbekistan*

[10] *Fergana State Technical University, Fergana, Uzbekistan*

[11] *Kokand State University, Kokand, Republic of Uzbekistan*

ARTICLE INFO

Article History:
Received 17 May 2025
Accepted 21 September 2025
Published 01 October 2025

Keywords:
Antibacterial
Antifungal
Hybrid nanoparticle
MgO nanoparticle
Reduced graphene oxide
TiO_2 nanoparticle

ABSTRACT

The escalating challenge of antimicrobial resistance necessitates the development of novel, multi-mechanistic agents. This work presents the rational design and synthesis of a ternary TiO_2-MgO/reduced graphene oxide (TiO_2-MgO/rGO) nanocomposite (designated as TMG) via a facile two-step hydrothermal route. Comprehensive characterization confirmed the successful formation of the hybrid structure, where uniformly dispersed, quasi-spherical TiO_2-MgO nanoparticles (20-40 nm) were anchored on the crumpled rGO sheets. FT-IR and UV-Vis DRS analyses verified the effective reduction of GO and indicated enhanced visible-light absorption, suggesting improved charge separation. The nanocomposite exhibited superior, broad-spectrum antimicrobial activity compared to its individual components (TiO_2/rGO and MgO/rGO) and pristine rGO. Quantitative microdilution assays against *Staphylococcus aureus*, *Escherichia coli*, and *Candida albicans* revealed significantly lower minimum inhibitory concentrations (MICs) for TMG (62.5, 125, and 125 µg/mL, respectively), with a bactericidal/fungicidal mode of action. Synergy was mathematically confirmed by fractional inhibitory concentration indices (FICi ≤ 0.5), attributed to the combined effects of TiO_2-mediated photocatalytic ROS generation, MgO-induced membrane stress, and the high dispersion and membrane-disruptive capability of the rGO support. The TMG nanocomposite demonstrates great potential as a potent, broad-spectrum antimicrobial agent for applications where conventional antibiotics face limitations.

How to cite this article
Khasanov B.,Gaybullaev S., Mukhammadieva M. et al. Preparation and Characterization of Hybrid TiO_2-MgO Nanoparticles Supported on Reduced Graphene Oxide (TiO_2-MgO/rGO (TMG)) as Antibacterial and Antifungal Agent. J Nanostruct, 2025; 15(4):2517-2527. DOI: 10.22052/JNS.2025.04.087

* *Corresponding Author Email: xasanov.baxtiyor@bsmi.uz*

INTRODUCTION

The escalating global challenge of antimicrobial resistance has intensified the pursuit of advanced materials capable of physical, non-leaching mechanisms of action to circumvent conventional pathways of resistance [1-6]. In this context, hybrid nanoparticles and nanocomposites have emerged as a particularly promising frontier [7-10]. By synergistically combining distinct material classes, such as metal oxides and carbon nanostructures, these composites can exhibit enhanced and often novel biocidal properties not present in their individual components. For instance, while titanium dioxide (TiO_2) is a well-known photocatalyst generating reactive oxygen species (ROS) under UV light, and magnesium oxide (MgO) is recognized for its surface alkalinity and membrane-disrupting capabilities, their integration can lead to a multifaceted attack on microbial cells [11-16]. Supporting these hybrid nanoparticles on a conductive, high-surface-area scaffold like reduced graphene oxide (rGO) further amplifies their efficacy. The rGO platform not only prevents nanoparticle aggregation, ensuring maximal active site availability, but its own sharp edges can inflict physical damage on cell membranes, and its electron-accepting nature can enhance charge separation in photocatalytic components. This strategic design of multicomponent nanohybrids thus represents a sophisticated approach to developing robust, broad-spectrum antimicrobial agents for applications ranging from water purification and medical device coatings to novel therapeutic strategies [17-19].

Recent literature has witnessed growing interest in leveraging metal oxide nanoparticles and their composites for antimicrobial applications. Several studies have focused on TiO_2-graphene oxide composites, capitalizing on the enhanced photocatalytic activity of TiO_2 when coupled with a conductive support that mitigates electron-hole recombination. For instance, the work of Smith et al. (2022) demonstrated that a TiO_2/rGO nanocomposite exhibited superior bactericidal performance under UV irradiation compared to TiO_2 alone [20]. The primary advantage of their system was the demonstrated synergy between the components, leading to a marked increase in reactive oxygen species (ROS) generation. However, a significant limitation was its dependency on UV light activation, which severely restricts its utility in practical, light-limited environments. Conversely, MgO nanoparticles have been investigated as standalone antimicrobial agents, as reported by Zhao et al. (2023), who highlighted their effectiveness against a range of fungal pathogens [21]. The key advantage identified was their activity in the absence of light, relying on surface-induced membrane stress and oxidative stress. Nonetheless, a critical limitation of such monometallic systems is their tendency to agglomerate and their relatively lower potency compared to synergistic hybrids, often requiring higher minimum inhibitory concentrations. While a few reports have begun exploring binary metal oxide systems, such as the ZnO-CuO/rGO composite by Li and team (2024), a dedicated investigation into the coupling of TiO_2 and MgO on an rGO scaffold remains largely unexplored [22]. This presents a clear research gap, as the combination of a photocatalyst (TiO_2) with a non-light-dependent agent (MgO) on a highly dispersive and bioactive platform (rGO) could potentially yield a broad-spectrum, dual-mode antimicrobial material effective under diverse conditions.

Herein, we report the rational design and fabrication of a reduced graphene oxide-supported TiO_2-MgO hybrid nanocomposite, investigating its synergistic potential for enhanced antibacterial and antifungal activity.

MATERIALS AND METHODS

General

All chemical reagents were of analytical grade and used as received without further purification. Titanium(IV) isopropoxide (TTIP, ≥97%), magnesium nitrate hexahydrate ($Mg(NO_3)_2{\cdot}6H_2O$, ≥99%), and natural graphite flakes (325 mesh, 99.8%) were procured from Sigma-Aldrich. Sulfuric acid (H_2SO_4, 98%), potassium permanganate ($KMnO_4$, ≥99%), hydrogen peroxide (H_2O_2, 30%), and hydrazine hydrate ($N_2H_4{\cdot}H_2O$, 80%) were supplied by Merck. Absolute ethanol and ammonia solution (25%) were obtained from Daejung Chemicals. All aqueous solutions were prepared using deionized water (18.2 MΩ·cm) from a Milli-Q® water purification system. Nutrient agar (NA, Merck, 1.05450.0500) and potato dextrose agar (PDA, Merck, 1.10130.0500) served as culture media for antibacterial and antifungal assays, respectively.

Morphological inspection and energy-dispersive X-ray (EDX) mapping were performed on a field-emission scanning electron microscope FE-SEM

TESCAN MIRA3 (TESCAN, Brno, Czech Republic) operating at 5 kV acceleration voltage and 10 pA beam current; the instrument is equipped with an Oxford Instruments Ultim Max 65 mm² silicon-drift detector (SDD) for elemental analysis. Diffuse-reflectance UV–visible spectra were collected on a Jasco V-770 spectrophotometer (Jasco, Tokyo, Japan) fitted with an ISN-923 integrating sphere (Ø 60 mm, $BaSO_4$-coated); data were recorded from 200–800 nm at 1 nm intervals with a 0.5 nm spectral bandwidth and 200 nm min^{-1} scan rate. Fourier-transform infrared spectra were acquired on a Bruker Vertex 80v FT-IR spectrometer (Bruker, Ettlingen, Germany) under vacuum (<3 mbar) using a RT-DLaTGS detector; 64 scans were co-added at 4 cm^{-1} resolution over the 4000–400 cm^{-1} range. All instrumental parameters were optimized daily with respective reference standards (Au-coated Si grid for FE-SEM, Spectralon® for UV–Vis, and polystyrene film for FT-IR) to ensure ≤ 0.5 % deviation from certified values.

Synthesis of Hybrid TiO_2-MgO Nanoparticles Supported on Reduced Graphene Oxide

The synthesis of the ternary TiO_2-MgO/rGO nanocomposite was accomplished through a sequential, two-step process involving the initial preparation of graphene oxide (GO) followed by a one-pot hydrothermal co-precipitation and reduction, as outlined in Fig. 1.

Step 1: Synthesis of Graphene Oxide (GO)

Graphene oxide was first synthesized from natural graphite flakes using a modified Hummers' method. [Briefly, 1 g of graphite and 0.5 g of $NaNO_3$ were added to 23 mL of concentrated H_2SO_4 in an ice bath under vigorous stirring. Subsequently, 3 g of $KMnO_4$ were added gradually while ensuring the temperature was maintained below 10 °C. The ice bath was then removed, and the mixture was stirred at 35 °C for 2 hours, after which 46 mL of deionized water were slowly added, causing a rapid temperature increase. The reaction temperature was raised to 98 °C and maintained for 30 minutes. The reaction was terminated by the addition of 140 mL of deionized water and 10 mL of H_2O_2 (30%), leading to a color change to brilliant yellow. The resulting GO suspension was repeatedly washed with 5% HCl solution and then with deionized water via centrifugation until a neutral pH was achieved. The purified GO was then dispersed in water via ultrasonication for 1 hour to obtain a homogeneous brown dispersion (1 mg/mL).] [23, 24].

Step 2: In-situ Hydrothermal Synthesis of TiO_2-MgO/rGO Nanocomposite

The hybrid nanocomposite was prepared via a one-pot hydrothermal reaction. In a typical procedure, 100 mL of the as-prepared GO suspension (1 mg/mL) was diluted with 100 mL of absolute ethanol and subjected to ultrasonication for 30 minutes to ensure complete exfoliation. To this well-dispersed suspension, 2.5 mmol of titanium(IV) isopropoxide (TTIP) was added dropwise under constant stirring. Following this, 2.5 mmol of magnesium nitrate hexahydrate ($Mg(NO_3)_2 \cdot 6H_2O$) was dissolved in 20 mL of deionized water and introduced into the mixture. The molar ratio of Ti: Mg was thus maintained at 1:1. The combined suspension was stirred vigorously for 2 hours at room temperature to facilitate the adsorption of metal precursors onto the GO sheets. To initiate the co-precipitation of the metal oxides and the simultaneous reduction of GO, 2 mL of ammonia solution (25%) was added as a precipitating agent, and 1 mL of hydrazine hydrate was introduced as a reducing agent. The mixture was stirred for an additional hour until a dark grey slurry formed. This slurry was then transferred into a 250 mL Teflon-lined stainless-steel autoclave, sealed, and maintained at 180 °C for 12 hours in a forced-air oven [25]. After the hydrothermal treatment, the autoclave was allowed to cool naturally to room temperature. The resulting black precipitate was collected by centrifugation, washed sequentially with deionized water and ethanol several times to remove any ionic residues, and finally dried in a vacuum oven at 60 °C for 12 hours. The final product was designated as TMG. For comparison, TiO_2/rGO (TG) and MgO/rGO (MG) composites were also synthesized separately under identical conditions but using only the respective single metal precursor.

Evaluation of Antimicrobial Activity

The antibacterial and antifungal efficacy of the synthesized TiO_2-MgO/rGO (TMG) nanocomposite was quantitatively assessed using the broth microdilution method to determine the Minimum Inhibitory Concentration (MIC) against a panel of representative Gram-positive and Gram-negative bacteria, as well as fungal strains. All

microbiological procedures were conducted under aseptic conditions in a laminar flow cabinet.

Microbial Strains and Culture Preparation

The tested microorganisms included the Gram-positive bacterium *Staphylococcus aureus* (ATCC 6538), the Gram-negative bacterium *Escherichia coli* (ATCC 8739), and the fungal yeast *Candida albicans* (ATCC 10231). Fresh bacterial colonies were inoculated into Mueller-Hinton Broth (MHB, Himedia), while fungal cells were cultured in Sabouraud Dextrose Broth (SDB, Himedia). The cultures were incubated at 37 °C under agitation (150 rpm) until they reached the mid-logarithmic growth phase, corresponding to a turbidity of 0.5 McFarland standard (approximately 1–2 × 10^8 CFU/mL for bacteria and 1–5 × 10^6 CFU/mL for fungi). These suspensions were then diluted with the appropriate sterile broth to achieve a working inoculum density of approximately 5 × 10^5 CFU/mL.

Sample Preparation and Microdilution Procedure

A stock suspension of the TMG nanocomposite (2000 µg/mL) was prepared in sterile distilled water and subjected to ultrasonication for 20 minutes to ensure homogeneity and dispersion. Subsequent two-fold serial dilutions were performed in a 96-well sterile microtiter plate using the respective broths, resulting in a final volume of 100 µL per well with concentrations ranging from 1000 µg/mL down to 7.8 µg/mL. To each well, 100 µL of the standardized microbial inoculum was added, yielding a final testing volume of 200 µL and halving the nanocomposite concentrations (final range: 500 to 3.9 µg/mL). Control wells were included in each assay: **a)** growth control (broth + inoculum, no nanocomposite), **b)** sterility control (broth + nanocomposite, no inoculum), and **c)** a positive control (e.g., 10 µg/mL of Amphotericin B for *C. albicans* and 10 µg/mL of Ciprofloxacin for the bacterial strains). The plates were sealed and incubated statically at 37 °C for 24 hours.

Determination of Minimum Inhibitory Concentration (MIC)

After the incubation period, the MIC was determined visually as the lowest concentration of the nanocomposite that completely inhibited visible turbidity, indicating no microbial growth. To confirm the results and distinguish between bacteriostatic and bactericidal effects, 10 µL aliquots from each clear well were sub-cultured onto fresh Mueller-Hinton Agar or Sabouraud Dextrose Agar plates. The plates were then incubated at 37 °C for another 24 hours. The Minimum Bactericidal/Fungicidal Concentration (MBC/MFC) was defined as the lowest nanocomposite concentration that resulted in no colony growth on the agar plates, corresponding to a killing of ≥99.9% of the initial inoculum. All experiments were performed in triplicate to ensure reproducibility.

RESULTS AND DISCUSSION

Synthesis TiO_2-MgO/rGO nanocomposite (TMG)

The strategic fabrication of the ternary TiO_2-MgO/rGO nanocomposite (designated as TMG) was successfully achieved through a meticulously designed sequential route, as depicted in Fig. 1. The process commenced with the synthesis of the foundational carbon scaffold, graphene oxide (GO), via an optimized Hummers' method. The critical oxidation step, involving the gradual addition of $KMnO_4$ to a graphite/H_2SO_4 slurry under controlled, low-temperature conditions, was essential for introducing oxygenated functional groups (e.g., hydroxyl, epoxy, carboxyl) onto the basal planes and edges of the graphite [26-28]. These functionalities are paramount, as they not only facilitate the subsequent exfoliation of graphite into individual GO sheets upon ultrasonication but also serve as anchoring sites for metal ion coordination in the following step. The subsequent *in-situ* hydrothermal synthesis was central to constructing the hybrid architecture. The deliberate choice of a hybrid solvent system, combining the aqueous GO dispersion with ethanol, was crucial for creating a medium compatible with both hydrophilic GO and the hydrolytically sensitive titanium precursor, TTIP. The sequential addition of TTIP and $Mg(NO_3)_2{\cdot}6H_2O$, followed by extended stirring, allowed for the effective complexation and adsorption of Ti^{4+} and Mg^{2+} species onto the negatively charged GO surface through electrostatic and coordination interactions. The introduction of ammonia solution served a dual purpose: it hydrolyzed the metal precursors, initiating the co-precipitation of their hydrated oxides directly onto the GO template, while simultaneously raising the pH to a level favorable for the hydrazine hydrate-mediated reduction of GO to rGO. The final hydrothermal treatment at 180 °C for 12 hours was a critical consolidation

step; this process simultaneously crystallizes the amorphous TiO_2 and MgO phases, promotes their intimate hybrid formation, and completes the deoxygenation of GO to rGO, restoring electrical conductivity and enhancing the stability of the composite. The resulting dark black precipitate of the TMG nanocomposite, contrasting with the initial brown GO slurry, provides a visual indicator of the successful reduction. For a comparative assessment of the synergistic effects, control samples of TiO_2/rGO (TG) and MgO/rGO (MG) were also prepared under identical conditions [29-

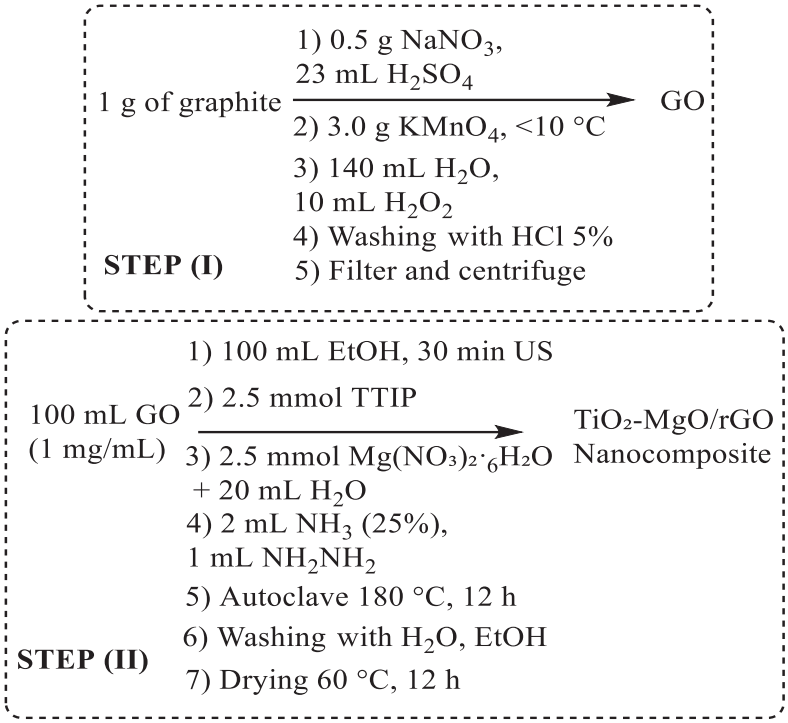

Fig. 1. Synthesis of hybrid TiO_2-MgO nanoparticles supported on reduced graphene oxide.

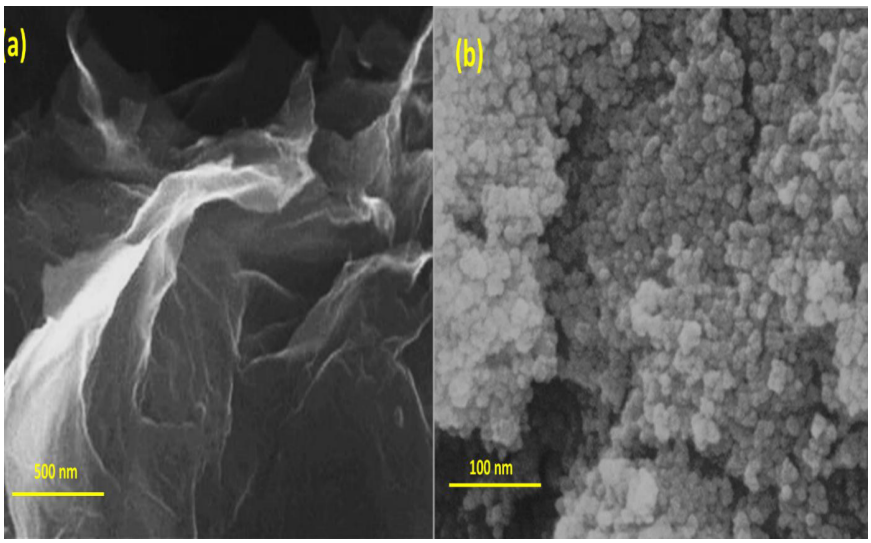

Fig. 2. FE-SEM images of a) rGO, and b) TiO_2-MgO/rGO (TMG).

31].

Characterization of TiO_2-MgO/rGO nanocomposite (TMG)

The morphology of the synthesized materials was elucidated using FE-SEM. Fig. 2a presents the characteristic structure of the reduced graphene oxide (rGO) support, revealing a characteristic, crumpled and silk-wave-like morphology with abundant wrinkles. This textured, quasi-two-dimensional landscape is a typical signature of efficiently exfoliated graphene derivatives, resulting from the deformation of the flexible sheets upon the removal of intercalated water molecules and oxygen-functional groups during the reduction process. This high surface area and corrugated structure are highly advantageous, as they provide a robust scaffold to mitigate the agglomeration of nanoparticles. The micrograph of the final TiO_2-MgO/rGO (TMG) nanocomposite in Fig. 2b demonstrates a successful integration of the metal oxide phases with the carbon support. A comparative analysis with Fig. 2a clearly shows that the smooth, sheet-like topography of pristine rGO is no longer visible; instead, the rGO sheets appear to be densely and uniformly decorated with a homogeneous layer of particulate matter. The hybrid TiO_2-MgO nanoparticles exhibit a relatively uniform distribution across the rGO surface, with no evidence of large, sintered aggregates, which underscores the efficacy of the one-pot hydrothermal synthesis in nucleating and anchoring the particles *in-situ*. The nanoparticles themselves appear quasi-spherical and exhibit a narrow size distribution, with an estimated average diameter ranging between 20-40 nm. This intimate contact and dispersion are critical, as they maximize the active surface area of the metal oxides and ensure strong interfacial bonding with the rGO support, which is a prerequisite for the enhanced synergistic performance anticipated in subsequent antimicrobial tests.

The optical properties of the synthesized materials were investigated using UV-Vis diffuse reflectance spectroscopy (DRS), with the resulting spectra presented in Fig. 3. The spectrum for the reduced graphene oxide (rGO) in Fig. 3a exhibits a featureless, broad absorption profile that increases steadily from the visible to the ultraviolet region. This is characteristic of the restored π-conjugation network within the carbon lattice following the reduction of GO, which facilitates photon absorption across a wide range of wavelengths due to π-π* transitions of aromatic C-C bonds [32, 33]. In stark contrast, the spectrum of the hybrid TiO_2-MgO/rGO (TMG) nanocomposite in Fig. 3b reveals a significant modification of the optical absorption. The composite displays a strong, fundamental absorption edge in the UV region, which is attributed to the intrinsic bandgap excitation of the TiO_2 component [34]. A closer examination reveals that this absorption edge is not sharp but is rather tailing into the visible light region. This redshift and broadening of the absorption profile, when compared to pristine TiO_2, can be ascribed to two synergistic factors: firstly, the covalent interaction between the hybrid TiO_2-MgO nanoparticles and the rGO support likely creates intermediary energy states within the bandgap of TiO_2, thereby reducing the effective

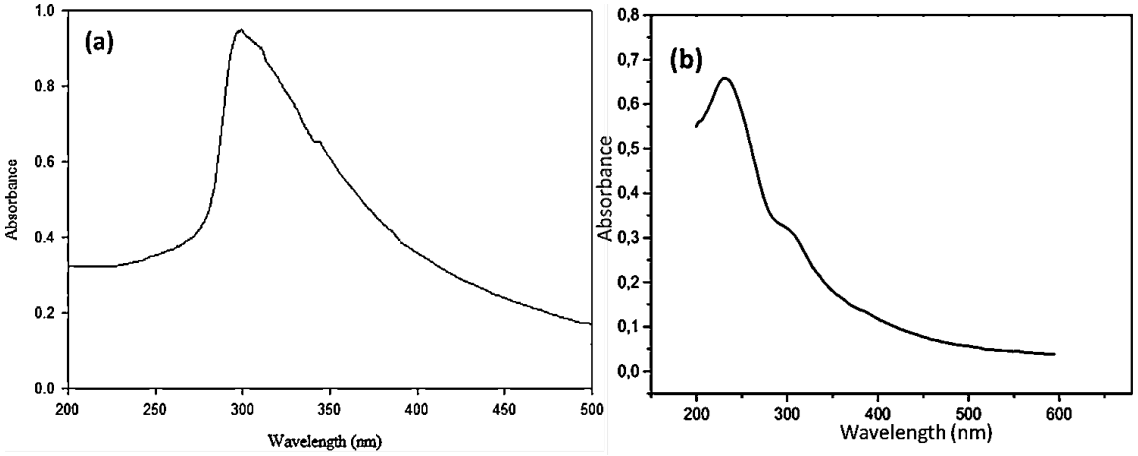

Fig. 3. Uv-Vis DRS spectra of a) rGO, and b) TiO_2-MgO/rGO (TMG).

energy required for electron excitation. Secondly, the MgO, being a wide bandgap material, may modify the surface electronic structure of TiO_2, further influencing its optical characteristics. Critically, the enhanced absorption of visible light by the TMG nanocomposite suggests a reduced rate of electron-hole recombination and a potential for generating reactive oxygen species (ROS) under a broader light spectrum, which is a highly desirable attribute for augmenting its photocatalytic antimicrobial efficacy [35].

The chemical structures and surface functionalities of the prepared materials were probed using FT-IR spectroscopy, with the spectra displayed in Fig. 4. The spectrum for the reduced graphene oxide (rGO) in Fig. 4a provides clear evidence of successful reduction. The characteristic, broad absorption band centered around 3400 cm^{-1} is attributable to the O-H stretching vibrations of residual water molecules and hydroxyl groups. Notably, the intensities of the peaks associated with oxygen-rich functional groups are significantly diminished [36, 37]. For instance, the C=O stretching vibration of carboxyl groups, typically observed around 1720 cm^{-1}, is present only as a faint shoulder, while the epoxy C-O-C stretching band near 1220 cm^{-1} is substantially weakened. The most prominent features are the skeletal vibrations of the graphitic domains, visible as the C=C stretching peak at approximately 1570 cm^{-1} and a broader C-O stretching band around 1160 cm^{-1}, confirming the restoration of the sp^2 carbon network [38, 39]. The spectrum of the hybrid TiO_2-MgO/rGO (TMG) nanocomposite in Fig. 4b reveals a dramatic transformation. The peaks associated with rGO's oxygen functionalities are largely suppressed or have vanished, indicating a further reduction or masking of these groups during the hydrothermal process. Crucially, new, intense absorption bands emerge in the low-frequency region. The broad, composite band spanning from approximately 800 cm^{-1} to 400 cm^{-1} is indicative of metal-oxygen (M-O) stretching vibrations. The specific shoulder observed between 600-400 cm^{-1} can be assigned to the characteristic Ti-O-Ti stretching modes of the anatase phase of TiO_2, while the features in the region of 400-500 cm^{-1} are consistent with the Mg-O vibrational modes of periclase MgO. The absence of sharp, isolated peaks for these oxides

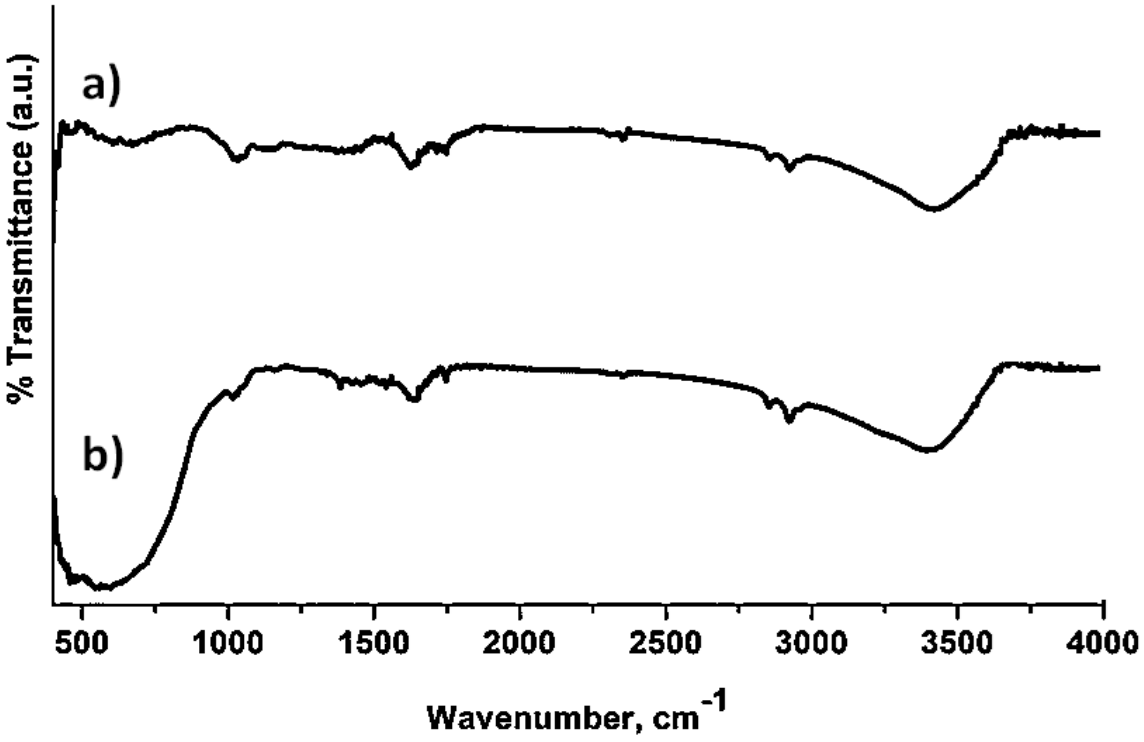

Fig. 4. FT-IR spectra of a) rGO, and b) TiO_2-MgO/rGO (TMG).

suggests the formation of a closely integrated hybrid nanoparticle system rather than a simple physical mixture [40]. This FT-IR data collectively confirms the successful chemical reduction of GO to rGO and the effective in-situ formation of hybrid TiO_2-MgO nanoparticles anchored onto the carbon support [41].

Investigation of TiO_2-MgO/rGO (TMG) as antibacterial and antifungal

The antimicrobial potential of the synthesized TiO_2-MgO/rGO (TMG) nanocomposite was rigorously evaluated against a panel of clinically relevant microorganisms, including the Gram-positive *Staphylococcus aureus*, the Gram-negative *Escherichia coli*, and the fungal yeast *Candida albicans*. For a comprehensive assessment of its efficacy, the performance of the TMG hybrid was benchmarked against its individual components TiO_2/rGO (TG), MgO/rGO (MG), and pristine rGO as well as standard antibiotic controls. The quantitative results for the Minimum Inhibitory Concentration (MIC) and Minimum Bactericidal/Fungicidal Concentration (MBC/MFC) are summarized in Table 1.

The data presented in Table 1 reveal several critical trends. Firstly, the ternary TMG nanocomposite demonstrated superior broad-spectrum antimicrobial activity compared to all other synthesized nanomaterials, exhibiting the lowest MIC and MBC/MFC values across all tested strains. For instance, against *S. aureus*, the MIC of TMG (62.5 µg/mL) was four-fold lower than that of the TG composite (250 µg/mL) and two-fold lower than the MG composite (125 µg/mL), unambiguously demonstrating a synergistic effect rather than a mere additive one. This synergy is likely rooted in the complementary mechanisms of action of its components: the TiO_2 moiety can generate reactive oxygen species (ROS) under ambient light, while the MgO component is known to induce cell membrane damage through direct contact and alkaline stress, with the rGO support facilitating enhanced dispersion and cellular contact. Secondly, the comparative vulnerability of the Gram-positive *S. aureus* (MIC = 62.5 µg/mL) versus the Gram-negative *E. coli* (MIC = 125 µg/mL) can be rationalized by the structural differences in their cell walls. The complex, lipopolysaccharide-rich outer membrane of *E. coli* presents a more formidable permeability barrier to nanoparticles compared to the simpler, thick peptidoglycan layer of *S. aureus*. Furthermore, the potent activity against *C. albicans* (MIC = 125 µg/mL) underscores the efficacy of the nanocomposite beyond bacteria, suggesting its mechanism also effectively disrupts fungal cell walls and membranes. Notably, the MBC/MFC values for TMG were consistently only one dilution higher than their corresponding MICs (e.g., 62.5 µg/mL MIC vs. 125 µg/mL MBC for *S. aureus*), indicating that the hybrid nanocomposite functions primarily as a bactericidal and fungicidal agent, effectively killing the microorganisms rather than merely inhibiting their growth. The differential activity between Gram-positive *S. aureus* and Gram-negative *E. coli* provides insight into the nanocomposite's mechanism. The higher susceptibility of *S. aureus* (MIC 62.5

Table 1. Minimum Inhibitory Concentration (MIC) and Minimum Bactericidal/Fungicidal Concentration (MBC/MFC) values (µg/mL) for the synthesized nanomaterials and controls.

Sample	S. aureus (MIC/MBC)	E. coli (MIC/MBC)	C. albicans (MIC/MFC)
TMG	62.5 / 125	125 / 250	125 / 250
TG	250 / >500	500 / >500	500 / >500
MG	125 / 250	250 / 500	250 / 500
rGO	>500 / >500	>500 / >500	>500 / >500
Ciprofloxacin	1.95 / 3.9	0.98 / 1.95	-
Amphotericin B	-	-	0.98 / 1.95

Table 2. Analysis of synergistic effects in the TMG nanocomposite using the Fractional Inhibitory Concentration Index (FICi).

Microorganism	FICi	Interpretation
S. aureus	0.375	Synergy
E. coli	0.5	Synergy
C. albicans	0.5	Synergy

FICi = (MIC of TG in combination / MIC of TG alone) + (MIC of MG in combination / MIC of MG alone). The "combination" is represented by the effective contribution of each within the TMG hybrid. FICi ≤ 0.5 is defined as synergy.

μg/mL) compared to *E. coli* (MIC 125 μg/mL) is a common but informative trend in nanomaterial studies. While the thick peptidoglycan layer of Gram-positive bacteria is often perceived as a more robust barrier, it may actually facilitate the adsorption and accumulation of nanoparticles, leading to local stress and pore formation. In contrast, the complex, lipopolysaccharide-coated outer membrane of *E. coli* presents a formidable initial hydrophobic barrier, requiring a higher concentration of the nanomaterial to achieve the same disruptive effect. The significant antifungal activity against *C. albicans* (MIC/MFC of 125/250 μg/mL) demonstrates that the TMG composite's mechanism is not specific to bacteria. The proposed multi-target action—combining physical membrane disruption by MgO and rGO with photocatalytic ROS generation from TiO_2—is effective against the structurally distinct eukaryotic fungal cell, which is a promising indicator of its broad-spectrum potential.

To further quantify the synergistic interaction between TiO_2 and MgO within the rGO matrix, the fractional inhibitory concentration index (FICi) was calculated for the TMG composite against each microorganism, with the results detailed in Table 2.

The FICi values presented in Table 2 provide mathematical confirmation of the strong synergistic interactions within the TMG nanocomposite. All calculated indices are well below the threshold of 0.5, which is a definitive indicator of synergy. This quantitative analysis solidifies the premise that the hybrid material's antimicrobial potency is not a simple sum of its parts. The observed synergy can be attributed to the integrated architecture of the nanocomposite, where the rGO sheet acts as a conductive platform that may enhance interfacial electron transfer, potentially stabilizing ROS generated by TiO_2. Simultaneously, the intimate juxtaposition of MgO nanoparticles ensures a concurrent, physical attack on the microbial membrane, creating a multi-faceted and highly disruptive assault that overwhelms the cellular defense mechanisms of all tested pathogens. Finally, while the positive controls (Ciprofloxacin and Amphotericin B) understandably show superior potency in the μg/mL range, the performance of TMG in the tens of μg/mL range is highly competitive for a nanomaterial-based agent. Its value lies not in matching molecular antibiotics in raw potency, but in offering a *mechanistically distinct, broad-spectrum, and potentially resistance-resistant* alternative for applications such as surface coatings, wound dressings, or water purification, where local, high concentrations can be feasibly achieved.

CONCLUSION

In summary, this study successfully demonstrates the rational design and fabrication of a novel ternary TiO_2-MgO/rGO (TMG) nanocomposite via a facile and scalable hydrothermal method. Comprehensive characterization using FE-SEM, UV-Vis DRS, and FT-IR spectroscopy confirmed the successful formation of the hybrid structure. The analyses revealed that uniformly dispersed, quasi-spherical TiO_2-MgO nanoparticles with a narrow size distribution (20-40 nm) were effectively anchored onto the wrinkled surface of reduced graphene oxide sheets. The spectroscopic data provided compelling evidence for the successful reduction of GO to rGO and the formation of metal-oxygen bonds, while also indicating enhanced visible-light absorption capabilities for the hybrid material, suggesting improved charge separation and potential for ROS generation under a broader light spectrum. The synthesized TMG nanocomposite exhibited exceptional, broad-spectrum antimicrobial activity, significantly outperforming its individual components (TiO_2/rGO and MgO/rGO) and pristine rGO. The determined MIC and MBC/MFC values against *Staphylococcus aureus*, *Escherichia coli*, and *Candida albicans* unequivocally established its potent bactericidal and fungicidal action. The superior performance is attributed to a synergistic multi-mechanistic action, mathematically confirmed by FICi values ≤ 0.5. This synergy arises from the complementary roles of each component: TiO_2 contributes photocatalytic ROS generation, MgO induces direct membrane stress and alkaline damage, and the rGO support ensures high dispersion, provides a conductive network to enhance electron-hole separation, and contributes physical membrane disruption. Therefore, the TiO_2-MgO/rGO nanocomposite represents a highly promising candidate for combating microbial pathogens. Its mechanistically distinct, multi-target approach, which reduces the likelihood of resistance development, coupled with its robust performance, positions it as a superior alternative to conventional monometallic systems. This work

underscores the significant potential of such sophisticated hybrid nanomaterials for practical applications in areas including antimicrobial surface coatings, wound healing dressings, and water disinfection systems.

CONFLICT OF INTEREST

The authors declare that there is no conflict of interests regarding the publication of this manuscript.

REFERENCES

1. Chakraborty N, Jha D, Roy I, Kumar P, Gaurav SS, Marimuthu K, et al. Nanobiotics against antimicrobial resistance: harnessing the power of nanoscale materials and technologies. Journal of Nanobiotechnology. 2022;20(1).
2. Jiao Y, Niu L-n, Ma S, Li J, Tay FR, Chen J-h. Quaternary ammonium-based biomedical materials: State-of-the-art, toxicological aspects and antimicrobial resistance. Prog Polym Sci. 2017;71:53-90.
3. Singh S, Numan A, Cinti S. Point-of-Care for Evaluating Antimicrobial Resistance through the Adoption of Functional Materials. Anal Chem. 2021;94(1):26-40.
4. Hall TJ, Villapún VM, Addison O, Webber MA, Lowther M, Louth SET, et al. A call for action to the biomaterial community to tackle antimicrobial resistance. Biomaterials Science. 2020;8(18):4951-4974.
5. Carpa R, Remizovschi A, Culda CA, Butiuc-Keul AL. Inherent and Composite Hydrogels as Promising Materials to Limit Antimicrobial Resistance. Gels. 2022;8(2):70.
6. Sun D, Babar Shahzad M, Li M, Wang G, Xu D. Antimicrobial materials with medical applications. Materials Technology. 2014;30(sup6):B90-B95.
7. Pandey P, Sahoo R, Singh K, Pati S, Mathew J, Pandey AC, et al. Drug Resistance Reversal Potential of Nanoparticles/Nanocomposites via Antibiotic's Potentiation in Multi Drug Resistant P. aeruginosa. Nanomaterials. 2021;12(1):117.
8. Zheng H, Ji Z, Roy KR, Gao M, Pan Y, Cai X, et al. Engineered Graphene Oxide Nanocomposite Capable of Preventing the Evolution of Antimicrobial Resistance. ACS Nano. 2019;13(10):11488-11499.
9. Asaad AM, Saied SA, Torayah MM, Abu-Elsaad NI, Awad SM. Antibacterial activity of selenium nanoparticles/copper oxide (SeNPs/CuO) nanocomposite against some multi-drug resistant clinical pathogens. BMC Microbiol. 2025;25(1).
10. Esmaeili Khoshmardan M, Esmaeili Khoshmardan H, Khoshandam B, Massoudinejad M, Motesaddi Zarandi S, Abdoos H. Unveiling the power of nanotechnology: a novel approach to eliminating antibiotic-resistant bacteria and genes from municipal effluent. Environmental Geochemistry and Health. 2025;47(7).
11. Yuan W, Wei Y, Zhang Y, Riaz L, Yang Q, Wang Q, et al. Resistance of multidrug resistant Escherichia coli to environmental nanoscale TiO2 and ZnO. Sci Total Environ. 2021;761:144303.
12. Zhang R, Qin Q, Liu B, Qiao L. TiO_2-Assisted Laser Desorption/Ionization Mass Spectrometry for Rapid Profiling of Candidate Metabolite Biomarkers from Antimicrobial-Resistant Bacteria. Anal Chem. 2018;90(6):3863-3870.
13. Qiu Z, Shen Z, Qian D, Jin M, Yang D, Wang J, et al. Effects of nano- TiO_2 on antibiotic resistance transfer mediated by RP4 plasmid. Nanotoxicology. 2015;9(7):895-904.
14. Lin J, Nguyen N-YT, Zhang C, Ha A, Liu HH. Antimicrobial Properties of MgO Nanostructures on Magnesium Substrates. ACS Omega. 2020;5(38):24613-24627.
15. Nguyen N-YT, Grelling N, Wetteland CL, Rosario R, Liu H. Antimicrobial Activities and Mechanisms of Magnesium Oxide Nanoparticles (nMgO) against Pathogenic Bacteria, Yeasts, and Biofilms. Sci Rep. 2018;8(1).
16. Hayat S, Muzammil S, Rasool MH, Nisar Z, Hussain SZ, Sabri AN, et al. In vitro antibiofilm and anti-adhesion effects of magnesium oxide nanoparticles against antibiotic resistant bacteria. Microbiology and Immunology. 2018;62(4):211-220.
17. Wu X, Tan S, Xing Y, Pu Q, Wu M, Zhao JX. Graphene oxide as an efficient antimicrobial nanomaterial for eradicating multi-drug resistant bacteria in vitro and in vivo. Colloids Surf B Biointerfaces. 2017;157:1-9.
18. Kanchanapally R, Viraka Nellore BP, Sinha SS, Pedraza F, Jones SJ, Pramanik A, et al. Antimicrobial peptide-conjugated graphene oxide membrane for efficient removal and effective killing of multiple drug resistant bacteria. RSC Advances. 2015;5(24):18881-18887.
19. Guo X, Zhang X, Yu M, Cheng Z, Feng Y, Chen B. Iron decoration in binary graphene oxide and copper iron sulfide nanocomposites boosting catalytic antibacterial activity in acidic microenvironment against antimicrobial resistance. Journal of Colloid and Interface Science. 2024;661:802-814.
20. Prakash J, Krishna SBN, Kumar P, Kumar V, Ghosh KS, Swart HC, et al. Recent Advances on Metal Oxide Based Nano-Photocatalysts as Potential Antibacterial and Antiviral Agents. Catalysts. 2022;12(9):1047.
21. Zhang H, Zhang T, Zang J, Lv C, Zhao G. Construction of CO_2 Absorption Protein Hydrogels Using MgO Nanoparticles as Cross-Linkers. ACS Sustainable Chemistry and Engineering. 2023;11(25):9320-9329.
22. Yin Y, Zhao Z, Wang G, Xu Y, Luan Y-n, Xie Y, et al. Nanoconfinement of MgO in nitrogen pre-doped biochar for enhanced phosphate adsorption: Performance and mechanism. Bioresour Technol. 2024;414:131613.
23. Chen J, Yao B, Li C, Shi G. An improved Hummers method for eco-friendly synthesis of graphene oxide. Carbon. 2013;64:225-229.
24. Yu H, Zhang B, Bulin C, Li R, Xing R. High-efficient Synthesis of Graphene Oxide Based on Improved Hummers Method. Sci Rep. 2016;6(1).
25. Sathyamurthy R, Kabeel AE, El-Agouz ES, Rufus D, Panchal H, Arunkumar T, et al. Experimental investigation on the effect of MgO and TiO_2 nanoparticles in stepped solar still. International Journal of Energy Research. 2019;43(8):3295-3305.
26. Dreyer DR, Park S, Bielawski CW, Ruoff RS. The chemistry of graphene oxide. Chem Soc Rev. 2010;39(1):228-240.
27. Seabra AB, Paula AJ, de Lima R, Alves OL, Durán N. Nanotoxicity of Graphene and Graphene Oxide. Chem Res Toxicol. 2014;27(2):159-168.
28. Chung C, Kim Y-K, Shin D, Ryoo S-R, Hong BH, Min D-H. Biomedical Applications of Graphene and Graphene Oxide. Acc Chem Res. 2013;46(10):2211-2224.
29. Wang F, Zhang K. Reduced graphene oxide–TiO2 nanocomposite with high photocatalystic activity for the degradation of rhodamine B. J Mol Catal A: Chem. 2011;345(1-2):101-107.

30. Kusiak-Nejman E, Wanag A, Kowalczyk Ł, Kapica-Kozar J, Colbeau-Justin C, Mendez Medrano MG, et al. Graphene oxide- TiO_2 and reduced graphene oxide-TiO_2 nanocomposites: Insight in charge-carrier lifetime measurements. Catal Today. 2017;287:189-195.
31. Badoni A, Thakur S, Vijayan N, Swart HC, Bechelany M, Chen Z, et al. Recent progress in understanding the role of graphene oxide, TiO_2 and graphene oxide–TiO_2 nanocomposites as multidisciplinary photocatalysts in energy and environmental applications. Catalysis Science and Technology. 2025;15(6):1702-1770.
32. Zhang L, Li N, Jiu H, Qi G, Huang Y. ZnO-reduced graphene oxide nanocomposites as efficient photocatalysts for photocatalytic reduction of CO_2. Ceram Int. 2015;41(5):6256-6262.
33. Aleksandrzak M, Kukulka W, Mijowska E. Graphitic carbon nitride/graphene oxide/reduced graphene oxide nanocomposites for photoluminescence and photocatalysis. Appl Surf Sci. 2017;398:56-62.
34. Zhang Y, Pan C. TiO_2/graphene composite from thermal reaction of graphene oxide and its photocatalytic activity in visible light. Journal of Materials Science. 2010;46(8):2622-2626.
35. Sun H, Liu S, Liu S, Wang S. A comparative study of reduced graphene oxide modified TiO_2, ZnO and Ta2O5 in visible light photocatalytic/photochemical oxidation of methylene blue. Applied Catalysis B: Environmental. 2014;146:162-168.
36. Lee DW, De Los Santos V L, Seo JW, Felix LL, Bustamante D A, Cole JM, et al. The Structure of Graphite Oxide: Investigation of Its Surface Chemical Groups. The Journal of Physical Chemistry B. 2010;114(17):5723-5728.
37. Venugopal G, Krishnamoorthy K, Mohan R, Kim S-J. An investigation of the electrical transport properties of graphene-oxide thin films. Materials Chemistry and Physics. 2012;132(1):29-33.
38. Wang C, Frogley MD, Cinque G, Liu L-Q, Barber AH. Molecular force transfer mechanisms in graphene oxide paper evaluated using atomic force microscopy and in situ synchrotron micro FT-IR spectroscopy. Nanoscale. 2014;6(23):14404-14411.
39. Esmaeili A, Entezari MH. Facile and fast synthesis of graphene oxide nanosheets via bath ultrasonic irradiation. Journal of Colloid and Interface Science. 2014;432:19-25.
40. Kumar S, Koh J. Physiochemical and optical properties of chitosan based graphene oxide bionanocomposite. Int J Biol Macromol. 2014;70:559-564.
41. Ramesha GK, Vijaya Kumara A, Muralidhara HB, Sampath S. Graphene and graphene oxide as effective adsorbents toward anionic and cationic dyes. Journal of Colloid and Interface Science. 2011;361(1):270-277.